Core-Shell NaHoF4@TiO2 NPs

Cui, Xianjin; Fryer, Benjamin; Zhou, Diwei; Lodge, Rhys W; Khlobystov, Andrei N; Valsami-Jones, Eugenia; Lynch, Iseult

DOI:
10.1021/acsami.9b03062

ACS APPLIED MATERIALS & INTERFACES

Research Article

Cite This: ACS Appl. Mater. Interfaces XXXX, XXX, XXX−XXX

www.acsami.org

Core−Shell $NaHoF_4$@TiO_2 NPs: A Labeling Method to Trace Engineered Nanomaterials of Ubiquitous Elements in the Environment

Xianjin Cui,*[,†] Benjamin Fryer,[†] Diwei Zhou,[§] Rhys W. Lodge,[‡] Andrei N. Khlobystov,[‡] Eugenia Valsami-Jones,[†] and Iseult Lynch[†]

[†]School of Geography, Earth and Environmental Science, University of Birmingham, Edgbaston, Birmingham B15 2TT, United Kingdom

[§]Department of Mathematical Sciences, University of Loughborough, Loughborough, LE11 3TU, United Kingdom

[‡]Nanoscale and Microscale Research Centre, Cripps South Building, University of Nottingham, Nottingham, NG7 2RD, United Kingdom

Supporting Information

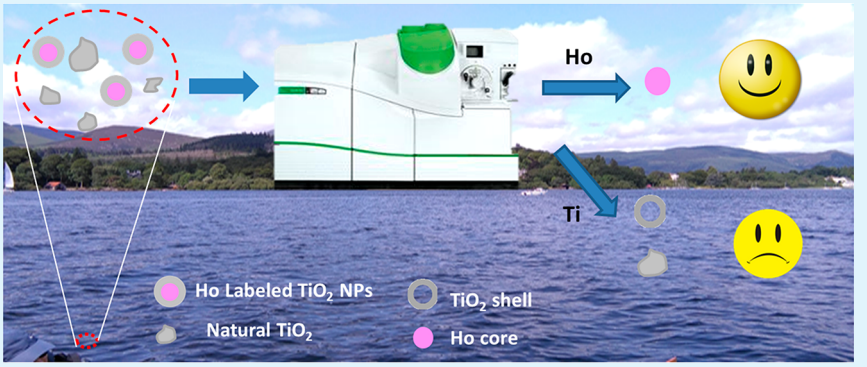

ABSTRACT: Understanding the fate and behavior of nanoparticles (NPs) in the natural environment is important to assess their potential risk. Single particle inductively coupled plasma mass spectrometry (spICP-MS) allows for the detection of NPs at extremely low concentrations, but the high natural background of the constituents of many of the most widely utilized nanoscale materials makes accurate quantification of engineered particles challenging. Chemical doping, with a less naturally abundant element, is one approach to address this; however, certain materials with high natural abundance, such as TiO_2 NPs, are notoriously difficult to label and differentiate from natural NPs. Using the low abundance rare earth element Ho as a marker, Ho-bearing core -TiO_2 shell ($NaHoF_4$@TiO_2) NPs were designed to enable the quantification of engineered TiO_2 NPs in real environmental samples. The $NaHoF_4$@TiO_2 NPs were synthesized on a large scale (gram), at relatively low temperatures, using a sacrificial $Al(OH)_3$ template that confines the hydrolysis of TiF_4 within the space surrounding the $NaHoF_4$ NPs. The resulting NPs consist of a 60 nm $NaHoF_4$ core and a 5 nm anatase TiO_2 shell, as determined by TEM, STEM-EDX mapping, and spICP-MS. The NPs exhibit excellent detectability by spICP-MS at extremely low concentrations (down to 1×10^{-3} ng/L) even in complex natural environments with high Ti background.

KEYWORDS: *spICP-MS, core−shell nanoparticles, large-scale synthesis, exposure and risk assessment, quantification*

INTRODUCTION

The past few decades have witnessed significant advances in nanotechnology, from the controlled synthesis of nanomaterials to their applications in nanomedicine,[1,2] energy harvesting and storage,[3,4] and soil and water remediation.[5,6] Nanosafety and nanotoxicology have emerged as new research topics in response to increasing concerns regarding the potential adverse effects on humans and the environment exposed to nanomaterials intentionally, or inadvertently.[7,8] As one of the few nanoparticles (NPs) that have already been widely used in industry for decades, TiO_2 NPs have been heavily produced for a wide range of applications, such as pigments, sunscreens, cosmetics, medical implants, self-cleaning surfaces, photovoltaics, photocatalysts, antifogging surfaces, and wastewater treatment.[9,10] Because of this prevalence, it is crucial to understand the fate of engineered TiO_2 NPs in the environment to assess their risk and control pollution. Indeed, TiO_2 NPs have been predicted to have the highest environmental occurrence of all engineered NPs, and have been found

Received: February 19, 2019
Accepted: May 6, 2019
Published: May 6, 2019

DOI: 10.1021/acsami.9b03062
ACS Appl. Mater. Interfaces XXXX, XXX, XXX−XXX

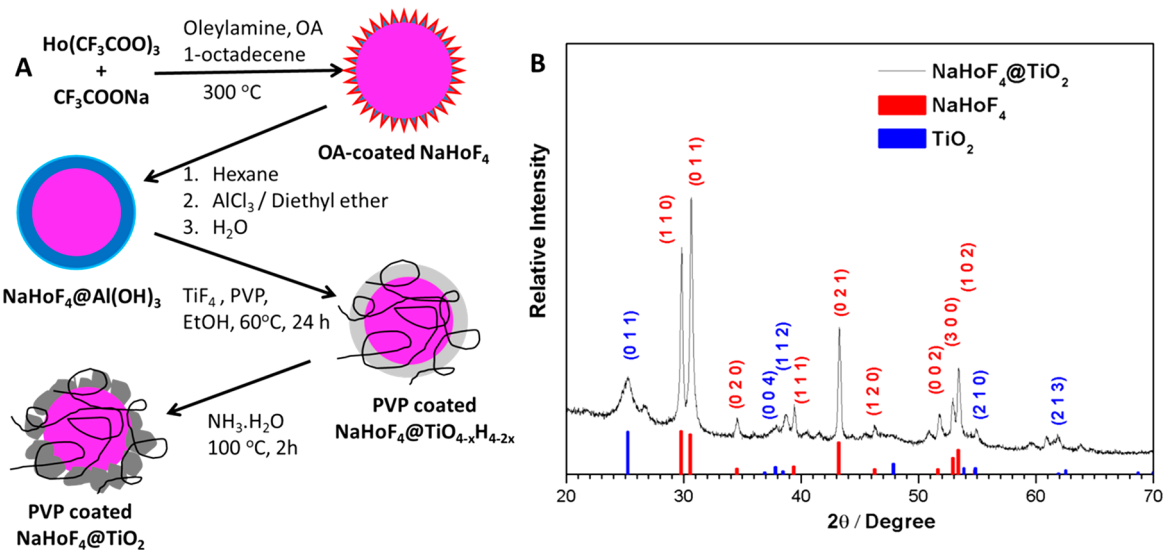

Figure 1. (A) A schematic illustration of the synthetic route to produce $NaHoF_4$@TiO_2NPs; and (B) X-ray powder diffraction pattern of $NaHoF_4$@TiO_2 NPs produced using an $Al(OH)_3$ template. $NaHoF_4$, JCPDS no. 00−049−1896; TiO_2, JCPDS no. 01−075−2545.

in treated wastewater, sewage sludge, surface waters, sludge-treated soils, and sediments.[11]

Environmental concentrations of Ti are strongly influenced by geogenic sources. In rivers with high concentrations of suspended matter (6.0−140.6 mg/L), the fraction of suspended Ti reached 62.3−88.6% (1.0−7.5 mg/g in terms of dry mass) with a strong correlation between the mass of suspended matter and the concentration of suspended Ti.[12] X-ray fluorescence spectrometry determined the Ti content of soil samples from Ti mining sites to range from 0.47 to 2.80%, but the Ti was found to be of geogenic origin with no anthropogenic input.[5] Though some efforts have been devoted very recently to discrimination of engineered TiO_2 from natural Ti-bearing NPs by a multielement detection approach,[13] this high natural background makes quantification of released and bioaccumulated concentrations of engineered TiO_2 NPs extremely challenging in the absence of some functionalization of the NPs to facilitate their discrimination. Labeling approaches proposed to date, for a range of NP compositions, have included radiolabeling,[14] stable isotope enrichment,[15] chemical doping with a low-abundance element,[16] or barcoding with DNA fragments.[17,18] Each of these potential approaches has advantages and challenges, with cost and the scale at which the NPs can be produced being the major drawback of all. For TiO_2 NPs, stable isotope labeling with ^{47}Ti has been successfully applied for detection of the bioaccumulation of NPs in zebra mussels (*Dreissena polymorpha*) exposed for 1 h at environmental concentrations via water (7−120 μg/L of $^{47}TiO_2$ NPs) and via their food (4−830 μg/L of $^{47}TiO_2$ NPs mixed with 1×10^6 cells/mL of cyanobacteria).[15] Chemical doping is a promising approach to achieve a large amount (grams compared to milligrams for radiolabeling) of labeled NPs at an affordable cost. However, introducing new cations into the lattice of host materials may alter their physical and chemical properties, even if the concentration of the dopant is low enough that the crystal structure remains unchanged.[19] It was reported that strong structural inhomogeneity, and even a phase transition, can be induced when there is a large difference in size between the substituted cations and the host cations.[20,21] A mixed-phase material, rather than a homogeneous solid solution, could be obtained because of unsuccessful doping. An alternative approach is to make a core of the tracer element surrounded by a shell of the material of interest. This core−shell approach is preferred for toxicological and environmental fate studies, because the material that comes into contact with the environment or living organisms will be the surface material and should be a close analogue of the undoped material, assuming that factors such as NP density are not significantly altered and appropriate crystal phase/morphology can be obtained.

ICP-MS was recently adopted as a means to detect NPs at ultra low concentration,[22] thanks to the capacity for element-specific analysis and the low detection limits (down to ng/L). However, ICP-MS fails to differentiate between engineered NPs composed of high abundance elements (e.g., Ti) and their natural counterparts.[23,24] To ensure that only engineered TiO_2 NPs are identified in complex media, Ho core−TiO_2 shell ($NaHoF_4$@TiO_2) NPs were synthesized with the low-abundance element Ho used as a chemical marker. The core−shell design was proposed to achieve a high dopant concentration for better detection while retaining the structural integrity of the NPs being investigated via the shell. $NaYF_4$ has been intensively investigated as a host for up-converting fluorescent materials with tunable particle sizes being demonstrated through the use of small NPs acting as nucleating seeds.[25] As an analogue of $NaYF_4$, it was expected that the size of $NaHoF_4$ NPs could be similarly controlled, to achieve particles above the size limit for spICP-MS detection (i.e., >20 nm).[24] For this reason, $NaHoF_4$ was selected as the marker core, although it is dissimilar from the TiO_2 shell both in structure and in composition.

TiO_2-coated NPs can be synthesized via a hydrothermal process,[26−29] or a sol−gel reaction on the NP surface,[30] and Caruso et al. even proposed a layer-by-layer method for coating TiO_2 onto polymer NPs.[31] Unfortunately, the hydrothermal conditions, or ultralow concentrations, make these approaches unfavorable for large-scale synthesis, a prerequisite for NPs for environmental studies. A sol−gel approach derived from the Stöber method has also been reported recently for TiO_2 coating;[32] however, this method was less effective for the coating of TiO_2 onto dissimilar

DOI: 10.1021/acsami.9b03062
ACS Appl. Mater. Interfaces XXXX, XXX, XXX−XXX

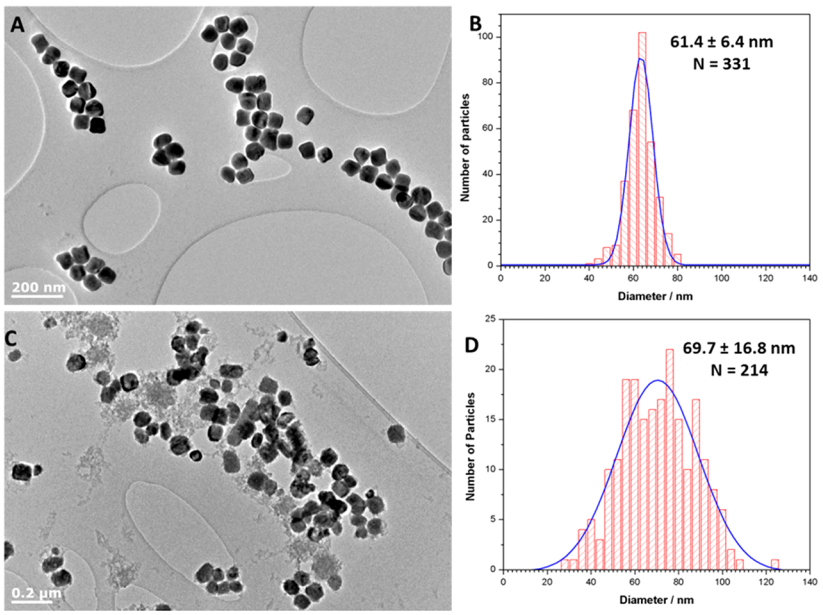

Figure 2. (A) TEM image and (B) size distribution of $NaHoF_4$ core NPs, (C) TEM image and (D) size distribution of $NaHoF_4$@TiO_2NPs. 331 $NaHoF_4$ NPs were counted for size analysis, yielding a median size and average size of 61.4 nm. 214 $NaHoF_4$@TiO_2 NPs were counted for size analysis, yielding a median size of 69.7 nm and an average size of 68.6 nm.

nanostructures[33] and a post-thermal treatment was needed to achieve a crystalline TiO_2 layer.

In this work, we developed a templating method for the large-scale synthesis of $NaHoF_4$@TiO_2 core−shell NPs, in which a sacrificial $Al(OH)_3$ layer was deposited onto the $NaHoF_4$ NP surface and then etched by HF or other fluorinated species via the hydrolysis of TiF_4.

RESULT AND DISCUSSION

The synthesis of $NaHoF_4$@TiO_2 NPs involved four steps (see the Experimental Section for further details). A typical procedure can be described briefly as follows. First, $NaHoF_4$ core NPs were obtained by thermolysis of $Ho(CF_3COO)_3$ and $NaCF_3COO$ in a mixed solvent consisting of a high boiling point solvent, 1-octadecene, and a coordinative solvent, oleylamine (Figure 1A), adapted from the approach published for $NaYF_4$ NPs and its analogues.[25] $Al(OH)_3$ was then deposited onto the $NaHoF_4$ NP surfaces to improve colloidal stability in polar solvents such as ethanol or water.[34] An aqueous solution of TiF_4 was introduced to the $NaHoF_4$@$Al(OH)_3$ NPs dispersion along with polyvinylpyrrolidone (PVP, M_w = 360 000) before the ethanol/water solvent system was heated to 60 °C with stirring and maintained at this temperature for 24 h. A subsquent addition of ammonia−water was followed by reflux at 100 °C for 2 h. Finally, the white product was isolated by centrifugation, washed with ethanol and water, and kept in ultrapure water.

The X-ray powder diffraction (XRD) pattern shown in Figure 1B confirmed the presence of hexagonal phase $NaHoF_4$ and tetragonal phase (anatase) TiO_2. Compared to the $NaHoF_4$ core NPs, however, an obvious broadening effect was observed for the TiO_2 phase, indicating a very small crystal size. Transmission electron microscopy (TEM) images in Figure 2 revealed a rough NP surface after coating with TiO_2, as well as an increase in the mean particle size from 61.4 to 68.6 nm. It was also noted that the size distribution of the NPs broadened, reflected by the fact that the standard deviation increased to 16.8 nm from 6.4 nm. Energy-dispersive X-ray (EDX) spectroscopy was utilized to further confirm the coexsitence of Ti and Ho (Figure S1, Supporting Information), as well as the core−shell structure of the NPs. Scanning transmission electron microscopy EDX (STEM-EDX) mapping allowed for the elemental distribution of the NPs to be determined. The elements from the $NaHoF_4$ core particle (F, Ho and Na) were observed to be encompassed by the Ti and O from the external TiO_2 shell (Figure 3A−F). In addition, more Ti was detected at the edges of the NP than in the core. Elemental line profiling was also done using STEM-EDX across a single core−shell NP to map its cross-sectional distibution of elements (Na, Ho, F, Ti and O). As observed in the elemental mapping, higher counts for Ti and O were detected at the periphery of the NPs (approximately 5 nm in thickness), while stronger signals from F and Ho from the $NaHoF_4$ core were evident in the middle of the NP, clearly demonstrating that the $NaHoF_4$ NPs were coated with a layer of TiO_2 (Figure 3G−L). A thickness of ca. 5 nm for the TiO_2 shell layer was consistent with the 9 nm increase in average particle size observed by TEM (Figure 2). Note that despite the use of an $Al(OH)_3$ template in this work, no Al was detected for the product of $NaHoF_4$@TiO_2 by EDX, as is evident from Figure 3.

$NaHoF_4$ NPs obtained in organic solvents could not be used directly for TiO_2 coating via a hydrolytic approach in ethanol, because they were inevitably covered by oleyamine and were thus dispersible only in nonpolar solvents; therefore, surface modification was required to make them dispersible in polar solvents. Additionally, there is a lack of interaction between the hydrophobic organic layer of the $NaHoF_4$NPs and the TiO_2 crystallite, which is unfavorable for the heterogeneous nucleation of TiO_2 on the $NaHoF_4$ surface.[35,36] The deposition of an $Al(OH)_3$ layer not only removes the surface bound oleylamine, but also imposes a highly positive surface charge onto the $NaHoF_4$ NPs,[34] providing a stable colloid in ethanol with a concentration up to 2 mg/mL. Once the TiF_4 solution was added into the NPs suspension, an external $Al(OH)_3$ layer

DOI: 10.1021/acsami.9b03062
ACS Appl. Mater. Interfaces XXXX, XXX, XXX−XXX

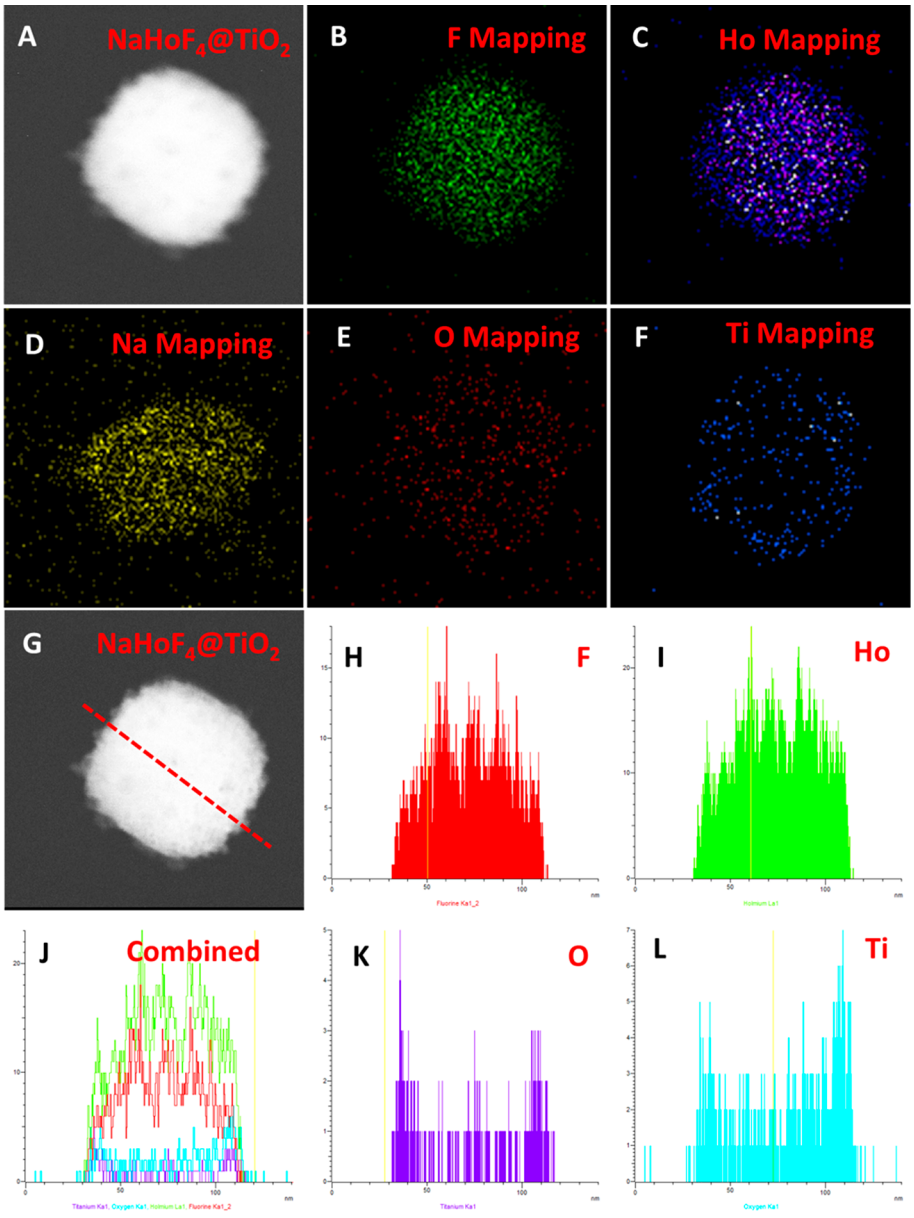

Figure 3. (A–F) STEM-EDX spectroscopy maps of an ~69 nm $NaHoF_4$@TiO_2 core–shell NP, confirming the coexistence of the Ho core and the TiO_2 shell, and (G–L) STEM-EDXline profiles of a $NaHoF_4$@TiO_2 NP highlighting the elemental distribution of the Ho and F core with the TiO_2 shell.

moves the equilibrium of hydrolysis toward the formation of $Ti(OH)_4$ by reacting with the consequential HF or through anion exchange with TiF_6^{2-}, TiF_5^- or other fluorinated species.[37] As a result, the $Al(OH)_3$ layer was etched and a Ti gel formed around the $NaHoF_4$NPs. Ammonia–water was subsequently introduced to catalyze the condensation of the Ti gel to form a TiO_2 layer on the NP surface. PVP was then used to protect the newly formed $NaHoF_4$@TiO_2 core–shell NPs from potential aggregation. A decrease in the hydrodynamic size was observed by dynamic light scattering (DLS) after the condensation triggered by addition of ammonia–water (Figure S2), thus confirming the loss of the $Al(OH)_3$ layer.

Some of the $NaHoF_4$@TiO_2 NPs showed a significantly different morphology and smaller size in comparison to the $NaHoF_4$ core NPs before coating (Figure S3), and particle size analysis by TEM also showed a broader size distribution after coating with TiO_2 (Figure 2). These results led to a hypothesis that $NaHoF_4$ NPs were not stable in the presence of H^+ or Al^{3+} since these ions could break Ho–F bonds, resulting in the formation of H–F or Al–F bonds.[37] This is supported by their bond dissociation energies (Al–F 675 kJ/mol, H–F 569 kJ/mol and Ho–F 540 kJ/mol). Increasing the temperature or polarity of the solvent would encourage the dissolution of $NaHoF_4$. Indeed, $NaHoF_4$ NPs appeared to be less stable in dimethyl sulfoxide (DMSO) than in ethanol. Only TiO_2 NPs were observed by TEM and a weak $NaHoF_4$ signal was detected by XRD for the product when using DMSO instead of ethanol as the solvent during the shell formation stage and on increasing the synthesis temperature to 160 °C (Figures S4 and S5).

Because of the intrinsic mismatch of the $NaHoF_4$ and TiO_2 lattices, TiO_2 tends to grow on the $NaHoF_4$ NP surface via a granule mode to form a rough layer consisting of small particles, minizing the free energy of system. As shown in the

DOI: 10.1021/acsami.9b03062
ACS Appl. Mater. Interfaces XXXX, XXX, XXX–XXX

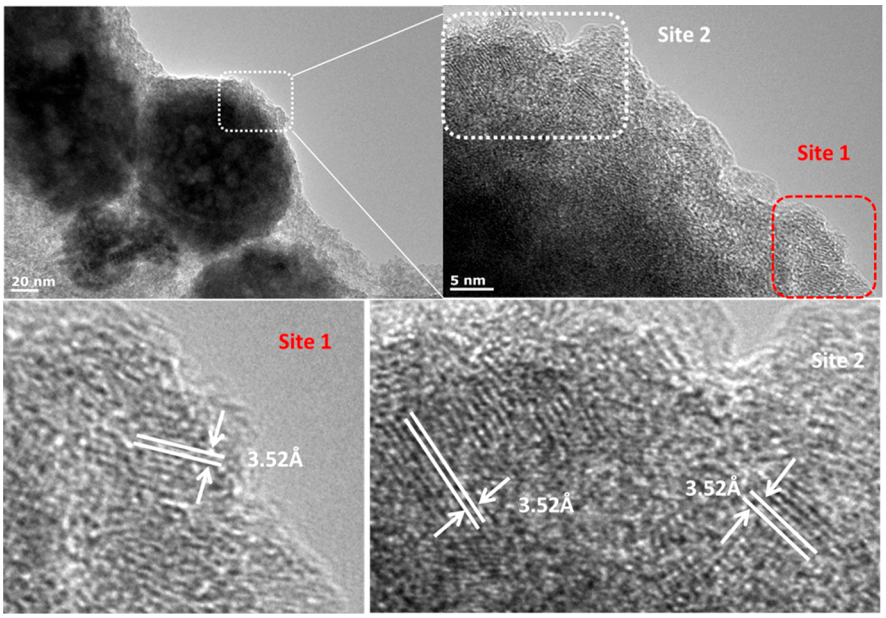

Figure 4. HRTEM images of $NaHoF_4$@TiO_2 core−shell NPs, showing the anatase phase of TiO_2 at the surface of the core−shell NPs.

Table 1. Summary of Synthetic Conditions and Scales for the Different Approaches Investigated for TiO_2 Coating of the $NaHoF_4$ Core NPs

entry	amount of core NPs	amount of ti precursor	conditions	ref
1	8.9 mg of Au	90 mL of 2.7 mmol/L TiF_4 aqueous solution	hydrothermal at 180 °C for 48 h	26
2	30 mg of α-Fe_2O_3	30 mL of 5.4 mmol/L TiF_4 aqueous solution	hydrothermal at 180 °C for 3 h	27
3	100 mg of $NaYF_4$(Yb, Tm)	28 mL of 5.7 mmol/L TiF_4 aqueous solution	hydrothermal at 180 °C for 3 h	28
4	10 mg of Cu_2O	25 mL of 0.3 mmol/L TiF_4 aqueous solution	hydrothermal at 180 °C for 0.5 h	29,41
5	2.7 mg of Ag	46 mL of 0.5 mmol/L Titanium tetraisopropoxide (TTIP) solution in ethanol	hydrolysis of TTIP in a mixture of H_2O and ethanol at room temperature for few minutes	29,30
6	1.9 mg of polystyrene	2 mL of 0.125 wt %Titanium bis (ammonium lactato) di- hydroxide solution	multisteps involved for coating TiO_2 on PS NPs, followed by calcining at 900 °C on N_2 for 4 h then on O_2 for 8 h	30,31
7	α- Fe_2O_3	100 mL of 40 mmol/L titanium butoxide solution in ethanol	stirring in ethanol for 18−24 h, followed by drying at 100 °C overnight and calcining at 500 °C for 2 h	32
8	SiO_2			
9	graphene oxide			
10	Fe_3O_4			
11	$NaYF_4$(Yb, Tm)/ Fe_3O_4	20 mL of 7.7 mmol/L titanium diisopropoxide bis(acetylacetonate) solution in ethanol	Stirring at 25 °C for 24 h, followed by drying at 60 °C and calcining at 500 °C for 3 h	33
12	1600 mg of $NaHoF_4$	800 mL of 31.3 mmol/L TiF_4 aqueous solution	in ethanol/water (740:60) at 60 °C for 2 h, then at 100 °C for 18 h	this work

TEM images (Figures 2C and 4), the $NaHoF_4$@TiO_2 core−shell NPs exhibited a rough surface after coating with TiO_2. High-resolution TEM images revealed that the outer TiO_2 layer is formed from small TiO_2 NPs with a size less than 5 nm. This is also reflected by the broadening of the diffraction peaks in the XRD pattern (Figure 1B). The (011) facets of TiO_2, with a *d*-spacing of 3.52 Å, were observed in HRTEM, and its corresponding diffraction peak at 25.3° appeared as the strongest peak in the XRD pattern, confirming the presence of anatase TiO_2. The bandgap of $NaHoF_4$@TiO_2 was determined as 3.7 eV (Figure S6), slightly larger than the typical value of 3.20 eV for anatase TiO_2, although this likely reflects the influence from the ultrasmall particle size of TiO_2.

The formation of a core−shell configuration is not only thermodynamically dependent on the interfacial energy between the core and shell materials but also sensitive to kinetic factors including the reaction rate, temperature and the amount of NPs serving as crystal seeds. Because of a lower critical free energy, heterogeneous nucleation requires a lower chemical potential than homogeneous nucleation.[35,38] In other words, a higher concentration (supersaturation) of the soluble crystallite is needed for homogeneous nucleation. Therefore, there is a concentration window to form the hybrid material, above the critical level for hetergeneous but below the level for homogeneous nucleation. As one specfic example of a hybrid material, $NaHoF_4$@TiO_2 NPs are more likely to form if the concentration of TiO_2 crystallite falls within this concentration window during the condensation process. Excess ammonia−water would lead to a fast condensation process, and a high concentration of TiO_2 crystallite if there are not enough $NaHoF_4$ NP seeds to consume them from the solution phase. Pure TiO_2 NPs, instead of core−shell structures, would form as a result of an homogeneous nucleation. However, an insufficient amount of ammonia could not trigger the

DOI: 10.1021/acsami.9b03062
ACS Appl. Mater. Interfaces XXXX, XXX, XXX−XXX

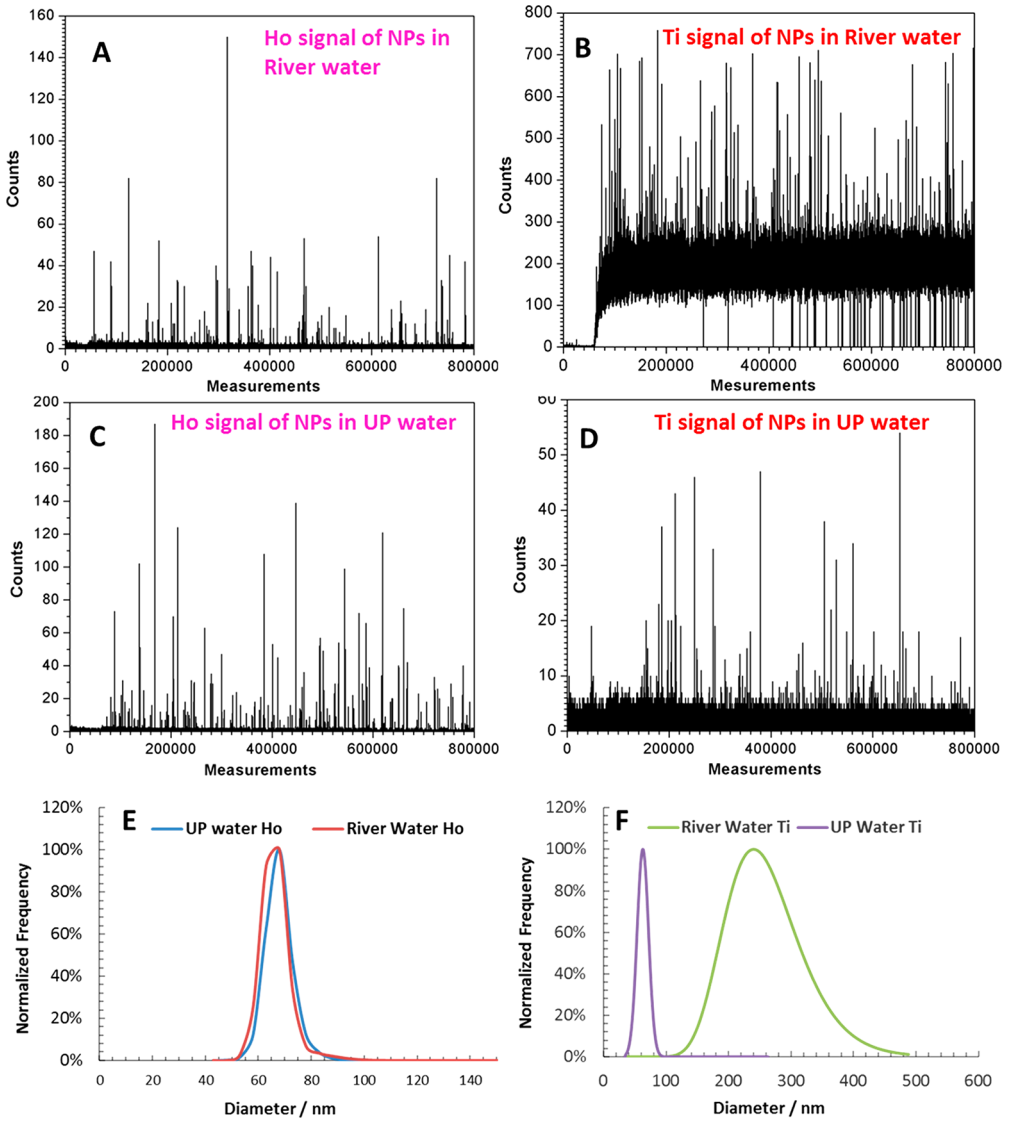

Figure 5. spICP-MS results of $NaHoF_4$@TiO_2 NP dispersions in ultrapure (UP) water and river water. (A) Real-time Ho signal from $NaHoF_4$@TiO_2 suspension in river water; (B) real-time Ti signal from $NaHoF_4$@TiO_2 suspension in river water; (C) real-time Ho signal from $NaHoF_4$@TiO_2 suspension in ultrapure water; (D) real-time Ti signal from $NaHoF_4$@TiO_2 suspension in ultrapure water; (E) size distribution of $NaHoF_4$ component detected by spICP-MS; and (F) size distribution of TiO_2 component detected by spICP-MS. Stock suspensions of NPs were diluted 100 million times with ultrapure water and river water, respectively, from ca. 1.5 mg/mL to ca. 15 ng/L for spICP-MS measurements. River water was collected from the Worcester and Birmingham Canal, near the University of Birmingham, and was used without filtration.

condensation or ensure a reasonable time scale for the reaction. Our results indicated that $NaHoF_4$@TiO_2 core–shell NPs can be obtained when the relative amounts of ammonia, ethanol and water are 2 mL:740 mL:60 mL, respectively. A mixture of $NaHoF_4$ NPs and ultrasmall TiO_2 particles was achieved if more than 2.5 mL of 35% ammonia–water was used (Figure S7). A colorless gel covered product was obtained if no or less than 1 mL of ammonia–water was added.

The challenges for synthesizing core–shell NPs on the scale required for field environmental fate experiments were thus to avoid the heterogeneous nucleation at a high concentration and the fact that a hybrid structure is thermodynamically less favorable than the formation of two separate homogeneous NPs. Unlike reactive Ti precursors, such as alkoxides, an elevated temperature or a high pH value is required to speed up the hydrolysis of TiF_4[39] or to facilitate the crystallization of TiO_2.. Currently, TiO_2-coated materials with improved crystallinity are typically synthesized by a hydrothermal approach with an extremely low concentration to avoid the formation of unwanted pure TiO_2 NPs at elevated temperatures[28,40] (Table 1). In this study, the $Al(OH)_3$ layer plays an important role when synthesizing $NaHoF_4$@TiO_2 NPs on a large scale. In addition to providing the NPs with excellent colloidal stability, it also serves as a sacrificial template to confine the hydrolysis and condensation process of TiF_4 to within the space surrounding the $NaHoF_4$NPs (Figure 1A), thereby helping to preclude the formation of pure TiO_2 NPs. The rate of TiF_4 hydrolysis was accelerated at a relatively low temperature (60 °C), without altering the pH value, because of the presence of the $Al(OH)_3$ layer preventing the condensation process. No product was isolated after the reaction was held at reflux for 24 h, in the absence of ammonia–water, and a gel-like product was recovered by centrifugation at 6000*g* for 20 min after stirring at 60 °C for 24 h following adjustment to a

DOI: 10.1021/acsami.9b03062
ACS Appl. Mater. Interfaces XXXX, XXX, XXX–XXX

pH of 4 (Figure S8), confirming the mechanism and the useful window for optimal core−shell NP synthesis.

Large-scale synthesis of TiO_2-coated NPs could be potentially achieved via a sol−gel approach,[32] despite the fact that a calcination process up to 500 °C is required to obtain a crystallized TiO_2 phase, with the consequent risk that larger particle aggregates may form because of the sintering effect. This approach requires preliminary NP seeds to be colloidally stable in a basic environment, which makes it inapplicable for positively charged or polymer-coated NPs. Positively charged NPs would lose their stability with addition of the ammonia−water catalyst, whereas NPs stabilized by functional polymer could remain colloidally stable in a basic environment, but the polymer layer being tightly bonded to the surface may hinder the coating with TiO_2 (Figure S9). PVP was used in this work, and it was expected to interact with NPs via weak van der Waals forces. Our results suggested that this losely bound polymer layer did not affect the TiO_2 coating. Because of the weak interaction between PVP polymer and the NPs, PVP can be readily removed by washing with water or replaced by other coatings (especially under highly alkaline conditions), allowing the surface to be made more representative of the TiO_2 particles used in food, commestics and other applications.[42,43]

As expected, the $NaHoF_4$@TiO_2 core−shell NPs indeed showed superior detectability on spICP-MS even in the presence of a high background of Ti up to the μg/L regime (Figure 5). Our results indicated that the ionic Ti levels in river (canal) water is up to 300 ppb, 100 times higher than the amount present in ultrapure water. In addition, Ti-containing particles were also observed in blank river water using spICP-MS. However, no Ho-containing particles, and very limited ionic Ho (<0.5 ppb), were detected either in river water or ultrapure water (Figure S10). To simulate the measurement conditions in an environmental study (e.g, quantification of release, accumulation, environmental transformations, or presence in effluent (or sludge) following treatment in a wastewater treatment plant, for example), we diluted the $NaHoF_4$@TiO_2 NP suspension (stock concentration, ca. 1.5 mg/mL) 100 million times with ultrapure water or river (canal) water, yielding a particle concentration of ca. 20 471 NPs/mL or a mass concentration of Ho of 4.5 ng/L as measured by spICP-MS. With the low background of Ti and Ho in ultrapure water, spICP-MS exhibited an excellent capacity to detect both the Ti and Ho components of the $NaHoF_4$@TiO_2 NPs, and mathematically provided an equivalent mean size (from the equivalent spherical volumes) of 68.0 and 54.8 nm for the $NaHoF_4$ core and TiO_2 shell, respectively (Figure 5E, F) using the density of anatase TiO_2 bulk material (3.9 g/cm^3) and a calculated density for $NaHoF_4$ (3.99 g/cm^3, see calculation in the Supporting Information). As the number of Ho- and Ti-containing particles detected were comparable, we can assume that the Ho and Ti components detected by spICP-MS come from the same core−shell NPs. This leads to an overall NP size of 78.2 nm for the $NaHoF_4$@TiO_2 NPs (Figure S11, see calculation in the Supporting Information), and subsequently a thickness of 5.1 nm for TiO_2 shell, which is very close to the value given by the size analysis of TEM images (4.2 nm) and by the element mapping by EDX (5 nm). Despite the slightly larger diameter achieved by spICP-MS than by TEM both for $NaHoF_4$ (68.0 nm vs 61.4 nm) and for $NaHoF_4$@TiO_2 (78.2 nm vs 69.7 nm), the results obtained by these two methods are convergent, if taking into account the fact that an underestimated value could be given by size analysis on TEM due to the low contrast (electron density) of TiO_2 and the nonspherical shape of particles, while an overestimated size could be yielded by spICP-MS if the actual density of the $NaHoF_4$ core is higher than the calculated value.

Not unexpectedly, spICP-MS was no longer able to detect the Ti component of the $NaHoF_4$@TiO_2 NPs in river water, because of the much higher abundance of background Ti than in ultrapure water (Figure 5A and B); however, the Ho component of $NaHoF_4$@TiO_2 NPs was easily detectable in the river water. Real signal intensity did not show much difference in river water or in ultrapure water, in terms of the frequency (particle number) and the intensity of the Ho peak (particle size) (Figure 5C, D). More importantly, the size of the Ho component (in the form of the $NaHoF_4$ core NP) detected under the different conditions (ultrapure water and river water) are the same, 68.0 nm (Figure 5E). A similar result was obtained across a wide $NaHoF_4$@TiO_2 NP concentration range both in ultrapure water and in river water (data now shown). In addition to the low abundance of the marker element (Ho), the long-term physical and chemical stability of the marker NP ($NaHoF_4$) is also crucial, because the leaching of Ho would result in an underestimated value for TiO_2 in the environmental samples. Only negligible ionic Ho (0.015 mg/mL) was detected in the suspension of $NaHoF_4$@TiO_2 NPs (*ca* 60−100 mg/mL), even after storage for over 14 months, which could be partially attributed to the core−shell structure, wherein the TiO_2 shell provides a barrier to the release of Ho.

These results demonstrated that spICP-MS is a sensitive and reliable technique to monitor Ti-containing NPs in complex environmental samples using Ho as a marker. This strategy could be extended to spICP-MS detection of NPs containing other nanomaterials containing elements of high natural abundance such as iron or zinc.

CONCLUSION

A novel approach to gram-scale synthesis of $NaHoF_4$@TiO_2 core−shell NPs was achieved, as a new strategy to detect NPs containing elements of high natural abundance such as Ti in complex environmental samples by spICP-MS. The deposition of an $Al(OH)_3$ layer around the Ho core was crucial for the synthesis of $NaHoF_4$@TiO_2 NPs, not only because of the excellent colloidal stability it provided in ethanol or water, but also because of the hydrophilic surface necessary for the effective TiO_2 deposition and coating. More importantly, the $Al(OH)_3$ layer acted as a sacrificial template which facilitated the separation of the hydrolysis and condensation of TiF_4 and confined these processes to the immediate vicinity of the $NaHoF_4$ NP surface, allowing for the deposition of the TiO_2 shell onto the $NaHoF_4$ NP surface. Even when using these approaches, the TiO_2 grew in a particular mode to form a noncontinuous phase on the $NaHoF_4$ NPs, which minimized the surface energy at the interface because of their mismatching lattice energies, resulting in $NaHoF_4$@TiO_2 NPs with rough surfaces. Although they were dissimilar in structure, the affinity of Ti to F is very high such that strong chemical interaction between TiO_2 and $NaHoF_4$ was expected and observed.

Due to the $Al(OH)_3$ layer, this approach allowed for the large scale synthesis of $NaHoF_4$@TiO_2 NPs, enabling their application in environmental studies of TiO_2 NP fate and behavior. The core−shell structure was confirmed by high-

DOI: 10.1021/acsami.9b03062
ACS Appl. Mater. Interfaces XXXX, XXX, XXX−XXX

resolution TEM and STEM-EDX mapping, as well as by spICP-MS. We demonstrated that these core−shell NPs remain detectable by spICP-MS in the presence of a high background of Ti despite the NPs being present at an extremely low concentration. The introduction of a low abundance element (Ho) as a tracer, without altering the structure of the particles, provided an effective solution for the detection of engineered TiO_2 NPs in the environment. This methodology will benefit research in nanotoxicology and ecotoxicology, and could also be a potential solution to the challenges of detecting other engineered NPs of high abundance elements such as Zn and Fe in the environment.

EXPERIMENTAL SECTION

Materials. All chemicals and solvents were purchased from Sigma Aldrich and used without further purification. Ultrapure water (18.2 MΩ cm at 25 °C) was obtained from a MiliQ purification system. River water was collected from the Worcester and Birmingham Canal near the University of Birmingham (UoB), and used immediately after collection without filtration.

Characterization and Synthesis of the NPs. Unless stated otherwise, all characterization was performed at UoB. X-ray powder diffraction data was collected on a Bruker D8 advance diffractometer with a copper target (λ = 1.5406 Å, 40 kV, 30 mA). All samples were prepared by drying 0.5 mL of aqueous solution onto an Si zero background holder in air. The parameters for a typical experiment are as follows: starting angle (2θ), 20°; stop angle, 80; step size, 0.02026°; time/step, 0.8 s; no. of scans, 3030; time of scanning, 42 min and 25 s. Hydrodynamic size and zeta potential were measured on a Zetasizer Nano ZS ZEN 3600 from Malvern. Single-particle ICP-MS (spICP-MS) data were obtained on a PerkinElmer NexION 350X. Transmission electron micropscopy (TEM), energy-dispersive X-ray (EDX) spectroscopy and elemental mapping were carried out at the Nanoscale and Microscale Research Centre, University of Nottingham on a JEOL2100F transmission electron microscope operating at 200 kV (field emission electron gun source, information limit 0.19 nm). EDX mapping was perfomed using an Oxford instruments XMax 80 T silicon drift detector with INCA Energy 250 Microanalysis system in conjunction with the JEOL digital STEM system.

Step 1: Synthesis of $NaHoF_4$ NPs. $Ho(CF_3COO)_3$ was obtained by dissolving Ho_2O_3 in trifluoroacetic acid (ca. 30% w/w) at 90 °C followed by removal of solvent on a rotary evaporator to obtain a pink powder. $Ho(CF_3COO)_3$ (8 mmol, 4.0 g) and $NaCF_3COO$ (11.8 mmol, 1.6 g) were dissolved in a 250 mL round-bottom flask containing oleayamine (40 mL) and 1-octadecene (40 mL) before being heated to 120 °C for 30 min in vacuo. After flushing with N_2 three times, 70 mL of the solution was removed by syringe and the rest of the solution in the flask was put on a preheated metal bath with stirring at 310 °C under an atmosphere of N_2. The 70 mL aliquot was slowly injected back into the system over a 30 min period with continuous stirring under N_2. Once all of the solution had been transferred, the temperature was lowered to 300 °C and the reaction system held at this temperature for 1 h before being cooled to room temperature. $NaHoF_4$ NPs precipitated from the solution by the addition of ethanol (200 mL), and were isolated by centrifugation prior to their redispersion in hexane (300 mL).

Step 2: Synthesis of $NaHoF_4$@$Al(OH)_3$ NPs. To the $NaHoF_4$ NP dispersion in hexane (300 mL), was added oleylamine (2 mL) with stirring at room temperature. The dispersion remained clear afterthe addition of a diethyl ether solution containing $AlCl_3$(5 mL, 1 g/mL). After stirring for 10 min, water (5 mL) was added dropwise, and the clear dispersion became more and more opaque to form a white cloudy but stable colloid. NPs were precipitated out by addition of acetone (300 mL), and collected by centrifugation.

Step 3: Synthesis of $NaHoF_4$@TiO_2 NPs. The $NaHoF_4$@$Al(OH)_3$ NPs were dispersed in ethanol (740 mL) in the presence of PVP (4 g, Mw = 360 000). An aqueous solution of TiF_4 (60 mL, 25 mmol) was quickly added into the ethanol dispersion of $NaHoF_4$@$Al(OH)_3$ NPs under stirring at 60 °C, resulting in a gradual color change from pink to a yellow-green within 5 min. After stirring at 60 °C overnight, the dispersion became slighly milky, indicating the formation of the Ti gel. The system was brought to reflux by heating to 100 °C. After the quick addition of ammonia−water (2 mL, 35% w/w), the solution became cloudy. A white product was achieved by centrifugation at 6000*g* for 30 min, which was subsequently washed with ethanol and water, and finally stored in water. The yield of $NaHoF_4$@TiO_2 NPs was calculated to be approximately 70% in terms of Ti.

spICP-MS Analysis of $NaHoF_4$@TiO_2 NPs. The NPs were diluted 100 million-fold using Milli-Q or canal water to obtain the final concentration for analysis. The dilution was chosen from a preliminary dilution test with dilution ranging from 10 000 to 10 000 000 000, from which it was found that 100 million-fold dilution brought the NP concentration to within 5000−200 000 particles mL^{-1} (this being the desired range for spICP-MS analysis). The elements within the NPs were analyzed sequentially, and the river (canal) water samples were run last in order to avoid any carryover effects that may occur due to the high background of Ti in the river water. The instrument was calibrated using PerkinElmer Setup Solution. Ti and Ho were calibrated using ionic solutions obtained from Aristar and PerkinElmer, prepared as a dilution series to form a calibration curve. Finally, the transport effiency was calculated using 20 and 40 nm gold NPs obtained from Nanocomposix and gold ionic solution from Aristar.

ASSOCIATED CONTENT

Supporting Information

The Supporting Information is available free of charge on the ACS Publications website at DOI: 10.1021/acsami.9b03062.

EDX, TEM images, element mapping, XRD, DLS, real-time signal of spICP-MS, and size calculation (PDF)

AUTHOR INFORMATION

Corresponding Author

*Email: x.cui@bham.ac.uk.

ORCID

Xianjin Cui: 0000-0003-0295-429X

Andrei N. Khlobystov: 0000-0001-7738-4098

Iseult Lynch: 0000-0003-4250-4584

Author Contributions

The manuscript was written through contributions of all authors. X.C. designed and carried out the synthesis and characterization of materials, analysized the data, and prepared the draft. B.F. and X.C. recorded and analyzed the spICP-MS results. D.Z. and X.C. analyzed the particle size and the size distribution. R.W.L., X.C., and A.N.K. carried out imaging and elemental analysis on TEM. I.L. and X.C. designed the study, I.L. and E.V.J. supervised the project, X.C. and I.L. wrote the first draft of the manuscript. All authors have given approval to the final version of the manuscript.

Funding

This work was supported by the European Union via the Horizon 2020 project NanoFASE (Grant 646002) and a Natural Environment Resaerch Council CASE PhD studentship with PerkinElmer as the CASE partner (BF).

Notes

The authors declare no competing financial interest.

ACKNOWLEDGMENTS

Intensive discussions with Ralf Keigi and Alexander Gogos (EAWAG) in terms of the NP specifications required for

DOI: 10.1021/acsami.9b03062
ACS Appl. Mater. Interfaces XXXX, XXX, XXX−XXX

quantification of TiO_2 NPs recovered from wastewater treatment plants (for example) within the NanoFASE project are gratefully acknowledged. The authors acknowledge the Nanoscale and Microscale Research Centre, University of Nottingham, for access to TEM facilities.

REFERENCES

(1) Wagner, V.; Dullaart, A.; Bock, A. K.; Zweck, A. The Emerging Nanomedicine Landscape. *Nat. Biotechnol.* **2006**, *24*, 1211−1217.
(2) Li, Y. P.; Lin, T. Y.; Luo, Y.; Liu, Q. Q.; Xiao, W. W.; Guo, W. C.; Lac, D.; Zhang, H. Y.; Feng, C. H.; Wachsmann-Hogiu, S.; Walton, J. H.; Cherry, S. R.; Rowland, D. J.; Kukis, D.; Pan, C. X.; Lam, K. S. A Smart and Versatile Theranostic Nanomedicine Platform Based on Nanoporphyrin. *Nat. Commun.* **2014**, *5*, 4712.
(3) Hu, L. B.; Choi, J. W.; Yang, Y.; Jeong, S.; La Mantia, F.; Cui, L. F.; Cui, Y. Highly Conductive Paper for Energy-storage Devices. *Proc. Natl. Acad. Sci. U. S. A.* **2009**, *106*, 21490−21494.
(4) Lu, H.; Peng, Y.; Ye, H.; Cui, X.; Hu, J.; Gu, H.; Khlobystov, A. N.; Green, M. A.; Blower, P. J.; Wyatt, P. B.; Gilin, W. P.; Hernandez, I. Sensitization, Energy Transfer and Infra-red Emission Decay Modulation in Yb^{3+}-doped $NaYF_4$Nanoparticles with Visible Light Through a Perfluoroanthraquinone Chromophore. *Sci. Rep.* **2017**, *7*, 5066.
(5) Maina, D. M.; Ndirangu, D. M.; Mangala, M. M.; Boman, J.; Shepherd, K.; Gatari, M. J. Environmental Implications of High Metal Content in Soils of a Titanium Mining Zone in Kenya. *Environ. Sci. Pollut. Res.* **2016**, *23*, 21431−21440.
(6) Suriyaraj, S. P.; Selvakumar, R. Advances in Nanomaterial Based Approaches for Enhanced Fluoride and Nitrate Removal from Contaminated Water. *RSC Adv.* **2016**, *6*, 10565−10583.
(7) Valsami-Jones, E.; Lynch, I. How Safe Are Nanomaterials? *Science* **2015**, *350*, 388−389.
(8) Oberdorster, G.; Oberdorster, E.; Oberdorster, J. Nanotoxicology: An Emerging Discipline Evolving from Studies of Ultrafine Particles. *Environ. Health Perspect.* **2005**, *113*, 823−839.
(9) Chen, X.; Mao, S. S. Titanium Dioxide Nanomaterials: Synthesis, Properties, Modifications, and Applications. *Chem. Rev.* **2007**, *107*, 2891−2959.
(10) Prieto-Rodriguez, L.; Miralles-Cuevas, S.; Oller, I.; Aguera, A.; Puma, G. L.; Malato, S. Treatment of Emerging Contaminants in Wastewater Treatment Plants (WWTP) Effluents by Solar Photocatalysis Using Low TiO_2 Concentrations. *J. Hazard. Mater.* **2012**, *211*, 131−137.
(11) Gottschalk, F.; Sonderer, T.; Scholz, R. W.; Nowack, B. Modeled Environmental Concentrations of Engineered Nanomaterials (TiO_2, ZnO, Ag, CNT, Fullerenes) for Different Regions. *Environ. Sci. Technol.* **2009**, *43*, 9216−9222.
(12) Linnik, P. N.; Zhezherya, V. A. Titanium in Natural Surface Waters: The Content and Coexisting Forms. *Russ. J. Gen. Chem.* **2015**, *85*, 2908−2920.
(13) Gondikas, A.; Von der Kammer, F.; Kaegi, R.; Borovinskaya, O.; Neubauer, E.; Navratilova, J.; Praetorius, A.; Cornelis, G.; Hofmann, T. Where is the Nano? Analytical Approaches for the Detection and Quantification of TiO_2 Engineered Nanoparticles in Surface Waters. *Environ. Sci.: Nano* **2018**, *5*, 313−326.
(14) Cui, X.; Green, M. A.; Blower, P. J.; Zhou, D.; Yan, Y.; Zhang, W.; Djanashvili, K.; Mathe, D.; Veres, D. S.; Szigeti, K. Al-$(OH)_3$Facilitated Synthesis of Water-soluble, Magnetic, Radiolabelled and Fluorescent Hydroxyapatite Nanoparticles. *Chem. Commun.* **2015**, *51*, 9332−9335.
(15) Bourgeault, A.; Cousin, C.; Geertsen, V.; Cassier-Chauvat, C.; Chauvat, F.; Durupthy, O.; Chanéac, C.; Spalla, O. The Challenge of Studying TiO_2 Nanoparticle Bioaccumulation at Environmental Concentrations: Crucial Use of a Stable Isotope Tracer. *Environ. Sci. Technol.* **2015**, *49*, 2451−2459.
(16) Ellis, L.-J. A.; Papadiamantis, A. G.; Weigel, S.; Valsami-Jones, E. Synthesis and Characterization of Zr- and Hf-doped Nano-TiO_2 as Internal Standards for Analytical Quantification of Nanomaterials in Complex Matrices. *R. Soc. Open Sci.* **2018**, *5*, 171884.
(17) Dahlman, J. E.; Kauffman, K. J.; Xing, Y. P.; Shaw, T. E.; Mir, F. F.; Dlott, C. C.; Langer, R.; Anderson, D. G.; Wang, E. T. Barcoded Nanoparticles for High Throughput *in vivo* Discovery of Targeted Therapeutics. *Proc. Natl. Acad. Sci. U. S. A.* **2017**, *114*, 2060−2065.
(18) Yaari, Z.; Da Silva, D.; Zinger, A.; Goldman, E.; Kajal, A.; Tshuva, R.; Barak, E.; Dahan, N.; Hershkovitz, D.; Goldfeder, M.; Roitman, J. S.; Schroeder, A. Theranostic Barcoded Nanoparticles for Personalized Cancer Medicine. *Nat. Commun.* **2016**, *7*, 7.
(19) Sharma, R. K.; Mudring, A. V.; Ghosh, P. Recent Trends in Binary and Ternary Rare-earth Fluoride Nanophosphors: How Structural and Physical Properties Influence Optical Behavior. *J. Lumin.* **2017**, *189*, 44−63.
(20) Teng, X.; Zhu, Y. H.; Wei, W.; Wang, S. C.; Huang, J. F.; Naccache, R.; Hu, W. B.; Tok, A. I. Y.; Han, Y.; Zhang, Q. C.; Fan, Q. L.; Huang, W.; Capobianco, J. A.; Huang, L. Lanthanide-Doped Na_xScF_{3+x} Nanocrystals: Crystal Structure Evolution and Multicolor Tuning. *J. Am. Chem. Soc.* **2012**, *134*, 8340−8343.
(21) Wang, F.; Han, Y.; Lim, C. S.; Lu, Y.; Wang, J.; Xu, J.; Chen, H.; Zhang, C.; Hong, M.; Liu, X. Simultaneous Phase and Size Control of Upconversion Nanocrystals Through Lanthanide Doping. *Nature* **2010**, *463*, 1061−1065.
(22) Mackevica, A.; Olsson, M. E.; Hansen, S. F. Silver Nanoparticle Release From Commercially Available Plastic Food Containers into Food Simulants. *J. Nanopart. Res.* **2016**, *18*, 11.
(23) Venkatesan, A. K.; Reed, R. B.; Lee, S.; Bi, X. Y.; Hanigan, D.; Yang, Y.; Ranville, J. F.; Herckes, P.; Westerhoff, P. Detection and Sizing of Ti-Containing Particles in Recreational Waters Using Single Particle ICP-MS. *Bull. Environ. Contam. Toxicol.* **2018**, *100*, 120−126.
(24) Lee, S.; Bi, X. Y.; Reed, R. B.; Ranville, J. F.; Herckes, P.; Westerhoff, P. Nanoparticle Size Detection Limits by Single Particle ICP-MS for 40 Elements. *Environ. Sci. Technol.* **2014**, *48*, 10291−10300.
(25) Cui, X. J.; Mathe, D.; Kovacs, N.; Horvath, I.; Jauregui-Osoro, M.; De Rosales, R. T. M.; Mullen, G. E. D.; Wong, W.; Yan, Y.; Kruger, D.; Khlobystov, A. N.; Gimenez-Lapez, M.; Semjeni, M.; Szigeti, K.; Veres, D.; Lu, H. Z.; Hernandez, I.; Gilin, W. P.; Protii, A.; Petik, K. K.; Green, M. A.; Blower, P. J. Synthesis, Characterization, and Application of Core Shell $Co_{0.16}Fe_{2.84}O_4$@$NaYF_4$(Yb, Er) and Fe_3O_4@$NaYF_4$(Yb, Tm) Nanoparticle as Trimodal (MRI, PET/SPECT, and Optical) Imaging Agents. *Bioconjugate Chem.* **2016**, *27*, 319−328.
(26) Wu, X. F.; Song, H. Y.; Yoon, J. M.; Yu, Y. T.; Chen, Y. F. Synthesis of Core-shell Au@TiO_2 Nanoparticles with Truncated Wedge-shaped Morphology and Their Photocatalytic Properties. *Langmuir* **2009**, *25*, 6438−6447.
(27) Lou, X. W.; Archer, L. A. A General Route to Nonspherical Anatase TiO_2 Hollow Colloids and Magnetic Multifunctional Particles. *Adv. Mater.* **2008**, *20*, 1853−1858.
(28) Qiu, Z. L.; Shu, J.; Tang, D. P. Near-infrared-to-ultraviolet Light-mediated Photoelectrochemical Aptasensing Platform for Cancer Biomarker Based on Core Shell $NaYF_4$:Yb, Tm@TiO_2 Upconversion Microrods. *Anal. Chem.* **2018**, *90*, 1021−1028.
(29) Liu, L.; Yang, W.; Sun, W.; Li, Q.; Shang, J. K. Creation of Cu_2O@TiO_2 Composite Photocatalysts with p-n Heterojunctions Formed on Exposed Cu_2O Facets, Their Energy Band Alignment Study, and Their Enhanced Photocatalytic Activity under Illumination with Visible Light. *ACS Appl. Mater. Interfaces* **2015**, *7*, 1465−1476.
(30) Sakai, H.; Kanda, T.; Shibata, H.; Ohkubo, T.; Abe, M. Preparation of Highly Dispersed Core/shell Type Titania Nanocapsules Containing a Single Ag Nanoparticle. *J. Am. Chem. Soc.* **2006**, *128*, 4944−4945.
(31) Caruso, F.; Shi, X. Y.; Caruso, R. A.; Susha, A. Hollow Titania Spheres From Layered Precursor Deposition on Sacrificial Colloidal Core Particles. *Adv. Mater.* **2001**, *13*, 740−744.
(32) Li, W.; Yang, J. P.; Wu, Z. X.; Wang, J. X.; Li, B.; Feng, S. S.; Deng, Y. H.; Zhang, F.; Zhao, D. Y. A Versatile Kinetics-Controlled Coating Method To Construct Uniform Porous TiO_2 Shells for

DOI: 10.1021/acsami.9b03062
ACS Appl. Mater. Interfaces XXXX, XXX, XXX−XXX

Multifunctional Core-shell Structures. *J. Am. Chem. Soc.* **2012**, *134*, 11864−11867.
(33) Lv, Y.; Yue, L.; Li, Q.; Shao, B. Y.; Zhao, S.; Wang, H. T.; Wu, S. J.; Wang, Z. P. Recyclable (Fe_3O_4-NaYF4:Yb, Tm)@TiO_2 Nanocomposites with Near-infrared Enhanced Photocatalytic activity. *Dalton Trans.* **2018**, *47*, 1666−1673.
(34) Cui, X. J.; Belo, S.; Kruger, D.; Yan, Y.; De Rosales, R. T. M.; Jauregui-Osoro, M.; Ye, H. T.; Su, S.; Mathe, D.; Kovacs, N.; Horvath, I.; Semjeni, M.; Sunassee, K.; Szigeti, K.; Green, M. A.; Blower, P. J. Aluminium Hroxide Stabilised $MnFe_2O_4$ and Fe_3O_4Nanoparticles as Dual-modality Contrasts Agent for MRI and PET Imaging. *Biomaterials* **2014**, *35*, 5840−5846.
(35) Thanh, N. T. K.; Maclean, N.; Mahiddine, S. Mechanisms of Nucleation and Growth of Nanoparticles in Solution. *Chem. Rev.* **2014**, *114*, 7610−7630.
(36) Sun, H.; He, J. T.; Wang, J. Y.; Zhang, S. Y.; Liu, C. C.; Sritharan, T.; Mhaisalkar, S.; Han, M. Y.; Wang, D.; Chen, H. Y. Investigating the Multiple Roles of Polyvinylpyrrolidone for a General Methodology of Oxide Encapsulation. *J. Am. Chem. Soc.* **2013**, *135*, 9099−9110.
(37) Buslaev, Y. A.; Dyer, D. S.; Ragsdale, R. O. Hydrolysis of Titanium Tetrafluoride. *Inorg. Chem.* **1967**, *6*, 2208−2212.
(38) Carbone, L.; Cozzoli, P. D. Colloidal Heterostructured Nanocrystals: Synthesis and Growth Mechanisms. *Nano Today* **2010**, *5*, 449−493.
(39) Gordon, T. R.; Cargnello, M.; Paik, T.; Mangolini, F.; Weber, R. T.; Fornasiero, P.; Murray, C. B. Nonaqueous Synthesis of TiO_2 Nanocrystals Using TiF_4 to Engineer Morphology, Oxygen Vacancy Concentration, and Photocatalytic Activity. *J. Am. Chem. Soc.* **2012**, *134*, 6751−6761.
(40) Zhang, N.; Liu, S. Q.; Fu, X. Z.; Xu, Y. J. Synthesis of M@TiO_2 (M = Au, Pd, Pt) Core-shell Nanoconnposites with Tunable Photoreactivity. *J. Phys. Chem. C* **2011**, *115*, 9136−9145.
(41) Wang, Z. Y.; Lou, X. W. TiO_2 Nanocages: Fast Synthesis, Interior Functionalization and Improved Lithium Storage Properties. *Adv. Mater.* **2012**, *24*, 4124−4129.
(42) Koczkur, K. M.; Mourdikoudis, S.; Polavarapu, L.; Skrabalak, S. E. Polyvinylpyrrolidone (PVP) in Nanoparticle Synthesis. *Dalton Trans.* **2015**, *44*, 17883−17905.
(43) Boopathi, S.; Senthilkumar, S.; Phani, K. L. Facile and One Pot Synthesis of Gold Nanoparticles Using Tetraphenylborate and Polyvinylpyrrolidone for Selective Colorimetric Detection of Mercury Ions in Aqueous Medium. *J. Anal. Methods Chem.* **2012**, *2012*, No. 348965.

DOI: 10.1021/acsami.9b03062
ACS Appl. Mater. Interfaces XXXX, XXX, XXX−XXX